



1 **Modeling of aerosol property evolution during winter haze**
2 **episodes over a megacity cluster in northern China: Roles of**
3 **regional transport and heterogeneous reactions**

4 Huiyun Du^{1,2}, Jie Li^{1,2,3*}, Xueshun Chen¹, Zifa Wang^{1,2,3}, Yele Sun^{1,2,3}, Pingqing Fu¹,
5 Jianjun Li⁴, Jian Gao⁵, Ying Wei^{1,2}

6 ¹ LAPC, Institute of Atmospheric Physics, Chinese Academy of Sciences, Beijing
7 100029, China

8 ² College of Earth Sciences, University of Chinese Academy of Sciences, Beijing
9 100029, China

10 ³ Center for Excellence in Urban Atmospheric Environment, Institute of Urban
11 Environment, Chinese Academy of Sciences, Xiamen, China

12 ⁴ China National Environmental Monitoring Center, Beijing, China

13 ⁵ Chinese Research Academy of Environmental Sciences

14 **Abstract.** Regional transport and heterogeneous reactions played crucial roles in haze
15 formation over a megacity cluster centered on Beijing. In this study, the updated Nested
16 Air Quality Prediction Model System (NAQPMS) and the HYSPLIT Lagrangian
17 trajectory model were employed to investigate the evolution of aerosols—in terms of
18 the number concentration, size distribution, and aging degree—in Beijing during six
19 haze episodes between November 15 and December 15, 2016, as part of the Air
20 Pollution and Human Health–Beijing (APHH–Beijing) winter campaign of 2016. The
21 model exhibited reasonable performance not only for mass concentrations of PM_{2.5} and
22 its components in Beijing but also for the number concentration, size distribution, and
23 aging degree. We discovered that regional transport played a nonnegligible role in haze
24 episodes, with contributions of 14%–31% to the surface PM_{2.5} mass concentration. The
25 contribution of regional transport to secondary inorganic aerosols was larger than that
26 of regional transport to primary aerosols (30%–63% vs. 3%–12%). The chemical
27 transformation of SO₂ in the transport pathway from source regions to Beijing was the
28 major form of SO₄²⁻ regional transport. We also found that sulfate formed outside
29 Beijing from SO₂ that was emitted in Beijing; this sulfate was then blown back to
30 Beijing and considerably influenced haze formation. In the transport pathway, aerosols



underwent aging, which altered the mass ratio of coating to black carbon (R_{BC}) and the size distribution of number concentrations. During the episodes, the geometric mean diameter (GMD) increased from less than 100 nm at the initial site to approximately 120 nm at the final site (Beijing), and R_{BC} increased from 2–4 to 4–8. These changes would affect regional radiation and climate. In haze episodes with high humidity, the average contributions of gas and aqueous chemistry, heterogeneous chemistry, and primary sulfate emission were comparable. Primary emissions had the greatest impact under light to moderate pollution levels, whereas heterogeneous chemistry had a stronger effect under high pollution levels.

Keywords: Regional transport; heterogeneous reactions; number size distribution; NAQPMS

1 Introduction

In past decades, a megacity cluster in China that is centered on Beijing and includes 28 cities (272,500 km², a population of 191.7 million people) has been experiencing frequent severe and persistent haze episodes (Zhao et al., 2013; Sun et al., 2014; Sun et al., 2016). PM_{2.5} levels exceeding 500 µg m⁻³ have often been reported. The adverse effects of PM_{2.5} on visibility, climate, and particularly human health have drawn widespread public attention (Hyslop, 2009; Chen et al., 2018; Yang et al., 2017a; Yang et al., 2017b; Anderson et al., 2010). Although the PM_{2.5} concentration in Beijing has decreased by 35% in the recent 5 years (2013–2017) because of implementation of the Atmospheric Pollution Prevention and Control Action Plan, the PM_{2.5} level in Beijing in 2017 still reached 58 µg m⁻³, which is 1.7 times the World Health Organization-recommended safe level of 35 µg m⁻³ (<http://www.bjepb.gov.cn/bjhrb/index/index.html>). Understanding the mechanism of haze episodes in this megacity cluster is thus an urgent task for policymakers.

Observations have revealed that haze episodes in this megacity cluster are mainly caused by the rapid formation of secondary inorganic species (SIA, including sulfate, nitrate, and ammonium) (Huang et al., 2014; Zheng et al., 2015; Han et al., 2016). The



59 SIA mass fraction in $\text{PM}_{2.5}$ can be up to 55% on days of severe pollution, which is 2.5
60 times that on clear days (Ma et al., 2017). Tang et al. (2016) proposed that local
61 chemical transformation related to humidity dominates the rapid formation of SIA in
62 Beijing. Yang et al. (2015) argued that local chemical conversion would not be fully
63 able to support the observed rapid formation of SIA in a short time. Using a ceilometer
64 and in situ observation data, Zhu et al. (2016) and Ma et al. (2017) further proposed
65 that regional transport was the major cause of the initial haze stage and that local
66 chemistry, particularly heterogeneous chemistry, dominated the later rise in Beijing.
67 This result is different from the findings obtained using numerical air quality models
68 (LOTOS-EUROS, Regional Air Quality Model System [RAQMS], and the Nested Air
69 Quality Prediction Modeling System [NAQPMS]) (Timmermans et al., 2017; Li and
70 Han, 2016; Li et al., 2017), in which regional transport dominated during haze episodes
71 in the megacity cluster. Recent observations of the physiochemical properties (e.g.,
72 mixing state, number concentration, and size distribution) of aerosols can provide more
73 information for improving the accuracy of regional transport and chemistry assessment.
74 Black carbon (BC) is usually more thickly coated by SIA and organic aerosols in
75 transported and aged air masses than in fresh particles, as indicated by the higher mass
76 ratio of coating to BC (R_{BC}) (Wang et al., 2018). Massoli et al. (2015) and Wang et al.
77 (2017) reported that R_{BC} exceeded 10 in remote sites after BC had undergone long-term
78 transport. This value was much higher than that in an urban area with high fresh particle
79 emissions, where R_{BC} generally was less than 1.5 (Liu et al., 2017). The geometric mean
80 diameter (GMD) of $\text{PM}_{2.5}$ also changed significantly due to the impact of regional
81 transport. In haze episodes in Beijing, the GMD increased to 120 nm in regionally
82 transported air masses, which is twice that under clean conditions (Ma et al., 2017).
83 Investigating the evolution of aerosol properties other than mass concentration during
84 regional transport is thus essential for assessing the roles of regional and local chemistry.
85 Such investigations are rarely conducted using the current three-dimensional chemical
86 transport models, which mostly concentrate on mass concentrations. The treatment of
87 heterogeneous chemistry is likely another source of modeling uncertainty. The current



88 models generally account for only a part of the observed SO_4^{2-} concentrations (Wang
89 et al., 2014). Heterogeneous chemistry is considered critical to improving model
90 performance (Zheng et al., 2015; Cheng et al., 2016; Li et al., 2018).

91 From November 15 to December 15, 2016, a field campaign was carried out in
92 Beijing within the framework of the UK-China Air Pollution & Human Health (APHH)
93 project. Nearly 30 Chinese and British institutions—including the Institute of
94 Atmospheric Physics, Chinese Academy of Sciences, Leeds University, the University
95 of Birmingham, the University of Reading, Tsinghua University, and Peking
96 University—participated in this campaign. Aerosol properties such as the size
97 distribution, number concentration, and mixing states were simultaneously measured in
98 China. APHH-Beijing aimed to explore the sources of and processes affecting urban
99 atmospheric pollution in Beijing. In the present study, we used the NAQPMS to
100 simulate aerosol properties in the campaign period as a part of the APHH winter
101 campaign. To improve model performance, the NAQPMS was updated by coupling it
102 with an advanced particle microphysics (APM) module that explicitly accounts for the
103 microphysical process and a new heterogeneous chemistry scheme (Chen et al., 2014;
104 Li et al., 2018). The hybrid single-particle Lagrangian integrated trajectory model
105 (HYSPLIT) was also employed to assess the evolution of aerosol properties (e.g.,
106 mixing state, number concentration, and size distribution). Crucially, the effects of
107 regional transport and heterogeneous chemistry on aerosol properties were quantified.
108 To the best of our knowledge, this is the first study to distinguish the contributions of
109 transport of SIA itself and its precursors to $\text{PM}_{2.5}$ in Beijing. We believe that this study
110 is helpful to understanding the causes of haze in this megacity cluster.

111 2 Model description and methodology

112 2.1 Model description

113 The Nested Air Quality Prediction Model System (NAQPMS) developed by the
114 Institute of Atmospheric Physics, Chinese Academy of Sciences (IAP/CAS) is a three-



dimensional Eulerian terrain-following chemical transport model. WRFv3.6.1, driven by Final Analysis (FNL) data from the National Centers for Environmental Prediction (NCEP), provides the meteorology field for the NAQPMS. The NAQPMS includes emission, horizontal and vertical advection and diffusion, dry and wet deposition, and chemical (including gas, aqueous, and heterogeneous) reaction processes (Wang et al., 2001; Li et al., 2012; Li et al., 2018). It also incorporates online source tagging, process analysis, an online WRF coupler, and other techniques (Wu et al., 2017; Wang et al., 2014). The Carbon Bond Mechanism version-Z (CBMZ) is used for gas-phase chemistry mechanisms. The thermodynamic model ISORROPIA1.7 is used to calculate the composition and phase state of an $\text{NH}_4^+ - \text{SO}_4^{2-} - \text{NO}_3^- - \text{Cl}^- - \text{Na}^+ - \text{H}_2\text{O}$ inorganic aerosol system (Nenes et al., 1998). Six secondary organic aerosols are managed using a two-product module. Further details of the NAQPMS can be found in the studies of Li et al. (2013, 2014, 2017), and numerous subsequent papers have been published describing recent updates.

To accurately describe aerosol properties (e.g., number concentration, size distribution, and mixing states), an advanced multitype, multicomponent, size-resolved microphysics (APM) module is coupled to the NAQPMS (Chen et al., 2014). APM explicitly describes microphysical aerosol processes, including nucleation, condensation, evaporation, coagulation, thermodynamic equilibrium with local humidity, hygroscopic growth, and dry and wet deposition (Yu and Luo, 2009), and it has already been applied in the global GEOS-Chem model (Ma et al., 2014). In the updated NAQPMS, 40 sectional bins covering 0.0012–12 μm were used to represent secondary particle distribution (SO_4^{2-} , NO_3^- , NH_4^+ , and secondary organic aerosols) (Chen et al., 2014). The size distribution of BC and primary organic aerosol was represented using 28 section bins. Other primary particles such as dust and sea salt were represented using four bins. The coating of secondary species on primary particles (sea salt, BC, OC, and dust) was explicitly simulated using a scheme that dynamically calculates the aerosol aging time with an hourly resolution on the basis of aerosol microphysics. The mass concentrations of coating species were also tracked in the



144 model. Chen et al. (2017) employed the updated NAQPMS and revealed that the
145 daytime aging time of BC in Beijing in winter can be less than 2 hours. This is much
146 less time than the fixed aging time scale of 1.2 days that has been stipulated in previous
147 studies (Liu et al. 2009) but is close to observed levels (2–4 hours) (Peng et al. 2016).
148 Li et al. (2018) further developed a heterogeneous chemical scheme based on mixing
149 states to reproduce the chemical transformation of gaseous precursors on an aerosol
150 surface, which largely altered the sizes and hygroscopicity of particles. Comparison
151 with long-term observations has proven that the updated NAQPMS can successfully
152 estimate aerosol mass and the number concentration, size distribution, mixing states,
153 and BC aging time in China (Li et al., 2017, 2018; Chen et al., 2014, 2017).

154 Distinguishing the contributions of the transport of SIA itself and its precursors to
155 PM_{2.5} is always difficult (Sun et al., 2014; Li et al., 2014, 2017; Ying et al., 2014). These
156 contributions have generally been named regional transport in studies; this leads to
157 ambiguity in regional transport. In this study, we divided the secondary species (e.g.,
158 SIA) in the i^{th} receptor region into four parts: 1) SIA locally produced from the i^{th} locally
159 emitted precursors (LC); 2) SIA chemically formed in other regions from the i^{th} locally
160 emitted precursors (LTC); 3) SIA chemically formed in the transport pathway to the i^{th}
161 receptor region of precursors emitted in the j^{th} source region (RTC); and 4) SIA
162 produced in the j^{th} region from precursors emitted in the j^{th} source region (RLC).

163 An online tracer-tagging module in the NAQPMS was used to resolve the
164 contributions from LC, LTC, RTC, and RLC. The module is capable of tracing both the
165 emission regions of precursors and the formation regions of secondary aerosols. First,
166 the mass contribution from the locations in which SIA was formed, called C_2 , was
167 tagged. The mass contribution from precursors emitted in different locations, called C_1 ,
168 was then tagged. More technical details can be found in the studies of Li et al. (2014)
169 and Wu et al. (2017). The following equation can be employed to calculate the degree
170 of chemical conversion during transport (TC):

$$171 \quad \text{TC} = \sum_{i=1}^n (C_{1i} - C_{2i} \times CC_i) \quad (1)$$

172 where C_{1i} refers to the absolute mass concentration transported to the receptor site,



173 produced by precursors emitted in region i ;
174 C_{2i} refers to the absolute mass concentration formed in region i and transported to
175 receptor site;
176 CC_i refers to the local contribution ratio of precursors in region i ;
177 $C_{2i} \times CC_i$ refers to the absolute mass transported to receptor site and generated at
178 region i by chemical conversion of precursors released at region i . When $i = 1$, it refers
179 to LC; when $i \neq 1$, $\sum_{i=2}^n C_{2i} \times CC_i$ refers to RLC;
180 $C_{1i} - C_{2i} \times CC_i$ is the mass concentration generated in all regions except i by chemical
181 conversion of the precursors released at region i and finally transported to the receptor
182 site. When $i = 1$, it refers to LTC; when $i \neq 1$, $\sum_{i=2}^n (C_{1i} - C_{2i} \times CC_i)$ refers to RTC.

183 In this study, 10 regions according to administrative division are selected for
184 source tagging (Fig. 1c), six of which—Chengde, Zhangjiakou, and Qinhuangdao
185 (NHB); Beijing (BJ); Tianjin (LT); Hengshui, Xingtai, and Handan (SHB); Baoding
186 and Shijiazhuang (WHB); and Tangshan, Langfang, and Cangzhou (EHB)—are a part
187 of the Beijing–Tianjin–Hebei (BTH) area. Henan (HN), Shandong (SD), Shanxi (SX),
188 and other regions (OT) are regions outside the BTH area.

189 2.2 Model structure

190 Simulation was conducted from November 10 to December 15, 2016, and the first
191 5 days were set aside as a spin-up period. The three nested model domains were shown
192 in Fig. 1a. The horizontal resolutions were 27, 9, and 3 km from the coarsest to
193 innermost domain. The first level of the NAQPMS was approximately 20 m in height,
194 and there were approximately 17 layers under 2 km.

195 To quantitatively assess the contribution of primary emissions, traditional
196 chemistry reactions (gas-phase and aqueous chemistry reactions), and heterogeneous
197 chemistry to sulfate, three sensitivity simulations were conducted. The baseline
198 scenario (Base) involving all heterogeneous reactions considered primary sulfate
199 emissions and its results were used for model verification and source apportionment
200 analysis. Control 1 (C1) involved all heterogeneous reactions but did not consider



201 primary sulfate emissions. Compared with Base, Control 2 (C2) excluded the
202 heterogeneous reactions of SO₂. Base–C2 represents the effect of heterogeneous
203 reactions on sulfate. Base–C1 represents primary sulfate emissions.

204 The HYSPLIT model was used to analyze the trajectories of air masses (Draxier
205 and Hess, 1998). The calculated trajectories are helpful to resolving the evolution of
206 aerosol properties in the transport pathway by extracting the simulated results by the
207 NAQPMS along trajectories. In this study, the same meteorology data (obtained hourly
208 data of the third domain) used in the NAQPMS were employed to perform trajectory
209 analysis; this avoided the errors caused by inconsistency between the two models (the
210 NAQPMS and HYSPLIT).

211 2.3 Emission inventory

212 The anthropogenic emissions were obtained from the 0.25° × 0.25° Multi-
213 resolution Emission Inventory for China (MEIC), and the base year was 2016 for BTH
214 (<http://www.meicmodel.org/publications.html>). In addition, observation data collected
215 at sites within BTH were used to update the MEIC on the basis of their latitude and
216 longitude information. Biomass burning emissions were taken from the Fire Inventory
217 from NCAR (National Center for Atmospheric Research) (Wiedinmyer et al., 2011).
218 Primary sulfate was assumed to constitute 5% of SO₂ emissions in the original MEIC
219 inventory, but through in situ measurement of source profiles, Cao et al. (2014), Wang
220 et al. (2009), Zheng et al. (2013), and Ma et al. (2015) discovered that primary sulfate
221 comprised approximately 40%, 6%, and 15% of primary PM_{2.5} from industrial, power,
222 and residential emissions, respectively, in the main form of (NH₄)₂SO₄. Thus, we
223 modified primary sulfate emissions in this study. Figure 1b displays the hourly primary
224 PM_{2.5} emission rate.

225 2.4 Observations

226 The surface meteorological parameters were obtained from the China
227 Meteorological Administration, whereas the vertical profiles of meteorological



parameters were obtained from the University of Wyoming
(<http://weather.uwyo.edu/upperair/sounding.html>). Observations of $\text{PM}_{2.5}$, SO_2 , NO_2 ,
and O_3 concentrations were obtained from the China National Environmental
Monitoring Center (<http://www.cnemc.cn/>). Aerosol components (including BC,
organic matters [OM], sulfate, nitrate, and ammonium) were measured in situ by using
an Aerodyne high-resolution time-of-flight aerosol mass spectrometer. Details of the
instruments can be found in the study by Sun et al. (2015). The particle number size
distributions at ground level was obtained using a scanning mobility particle sizer
(SMPS) with a time resolution of 5 min. Details of the instruments can be found in the
study by Du et al. (2017). All data in this study are presented in Beijing local time (UTC
+ 8 h).

3 Model validation

3.1 $\text{PM}_{2.5}$ mass and number concentrations and aging degrees

The time series of simulated and observed $\text{PM}_{2.5}$ in different cities of BTH from
November 15 to December 15, 2016, are illustrated in Fig. 2. In the study period, six
regional haze episodes were identified, namely, November 15–20 (Ep1), November 23–
26 (Ep2), November 28–30 (Ep3), December 2–4 (Ep4), December 6–8 (Ep5),
December 10–12 (Ep6). The $\text{PM}_{2.5}$ mass concentration frequently exceeded $200 \mu\text{g m}^{-3}$
and the average concentration reached $120 \mu\text{g m}^{-3}$ during episodes. Haze usually
formed in several hours; for example, the increasing rate of $\text{PM}_{2.5}$ reached $200 \mu\text{g m}^{-3}$
 h^{-1} and lasted approximately 12 hours in Tangshan. These observed haze patterns were
generally reproduced by the NAQPMS. The correlation coefficient (R) between the
observation and simulation in most cities was 0.6–0.8, and 60%–80% of simulation
results were within a factor of 2 of the observation. The mean fractional bias (MFB)
and mean fractional error (MFE) ranged from -0.07 to 0.7 , meeting the criteria of MFB
 ≤ 0.6 and $\text{MFE} \leq 0.75$ (Boylan et al., 2006). The simulation did however underestimate
 $\text{PM}_{2.5}$ in Beijing and Baoding for Ep2. This was caused by the failure of the mineral



255 aerosol transport simulation. Compared with other cities in the cluster, Beijing and
256 Baoding are closer to the Gobi Desert, a major dust source in East Asia, and they are
257 thus more easily affected by dust storm transport. Pan *et al.* (2018) found a pronounced
258 peak in the size distribution at 4–5 μm for Ep2 in Beijing. The concentrations of Ca^{2+}
259 was 7 times the campaign averages (Fig. S1).

260 The aerosol components in Beijing, Langfang, and Baoding are compared in Fig.
261 3. In general, the simulation largely reproduced the variation in primary and secondary
262 aerosols. In particular, the rapid increase in SIA during Ep1, Ep2, and Ep4 was captured
263 by the simulation. Interestingly, the NAQPMS underestimated the sulfate concentration
264 in Beijing during Ep2 and Ep4, but the nitrate and ammoniate concentrations during
265 these two episodes were successfully reproduced. This was related to the transport of
266 mineral dust (Ep2) and local emissions (Ep4). As discussed in the last paragraph,
267 Beijing had high mineral loadings for Ep2, which provided a favorable medium for
268 chemical transformation of anthropogenic SO_2 into sulfate in the form of CaSO_4 or
269 MgSO_4 (Zhuang *et al.*, 1992). Underestimation of the sulfate concentration for Ep4 may
270 have been caused by local emissions in Beijing. As illustrated in Fig. 3, the simulation
271 failed to reproduce the sharp increase in both sulfate and BC in Beijing during this
272 episode. This is different from the case of Ep2, in which sulfate was underestimated but
273 BC was favorably reproduced. Wang *et al.* (2009) and Ma *et al.* (2015) found that sulfate
274 accounted for 40% and 6.6% of primary $\text{PM}_{2.5}$ emissions from industry and power
275 plants, which also emit a large amount of BC. This sharp increase in BC was a local-
276 scale episode. In Langfang, a site 50–60 km from Beijing, both the observed and
277 simulated BC concentration increased slowly to $20 \mu\text{g m}^{-3}$, which is much less than that
278 in Beijing ($45 \mu\text{g m}^{-3}$). The monthly emissions employed in this study made it difficult
279 to capture these short-term local-scale emission changes. The simulated SO_2 and NO_2
280 concentrations are compared with the observations in Fig. S2, and the normalized mean
281 bias (NMBs) of these concentrations were less than 40%.

282 The number size distribution is critical to examining aerosol evolution during haze
283 episodes (Ma *et al.*, 2017). In this study, both the simulation and observation revealed



284 a rapid increase in the GMD from 50 to approximately 120 nm during the initial stages
285 of episodes in Beijing (Fig. 4). The observed mean number concentration of aerosols
286 ($dN/d\log D_p$) showed a unimodal distribution and was mainly concentrated in the
287 Aitken mode (25–100 nm) and accumulation mode (100–1,000 nm). The highest
288 concentration was approximately $1.8 \times 10^4 \text{ cm}^{-3}$ at a 100-nm diameter. These patterns
289 were favorably reproduced by the simulation. The simulated number concentrations
290 were underestimated in 10–60 nm by 20%–30% and overestimated in 80–150 nm by
291 20%. This indicated that the model needs to be improved regarding its treatment of new
292 particle formation and the volatility of primary organic aerosols.

293 Herein, the aging degree of BC is represented by the mass ratio of coating to BC
294 (R_{BC}), which has been widely used in previous studies (Oshima et al., 2009; Collier et
295 al., 2018). Figure 11 shows that the mean simulated R_{BC} in Beijing was 4.5 and 5.0 in
296 the entire study period and during pollution episodes, respectively, which are extremely
297 close to the observations (~ 5.0 and 5.1) (Wang et al., 2018). The high performance of
298 the model in terms of mass and number concentrations, compositions, and the mixing
299 state of aerosols gives us confidence for analyzing aerosol evolution during transport
300 in the megacity cluster centered on Beijing.

301 3.2 Meteorology

302 The simulated wind direction and speed coincided with the observations for the
303 haze episodes. In particular, the model captured low wind speeds, and the times at which
304 the wind shifted direction were well reproduced (Fig. S3). Regarding relative humidity
305 and temperature, WRF performed high values of R (0.68–0.93) and low NMBs (-0.51
306 to 0.44) (Table S1). In particular, the high relative humidity during Ep1 was well
307 reproduced. Inversion layers were present during the initial stage of haze formation (Fig.
308 S4). The height of the inversion layers varied among episodes. During Ep1 and Ep6,
309 strongly elevated inversion layers were present between 1 and 2 km, whereas the
310 inversion layers were close to the surface during other episodes. Temperature inversion
311 is favorable for pollution accumulation, and the model reproduced this feature favorably.



312 In sum, the high performance of the meteorological simulation gave us confidence for
313 PM_{2.5} simulation.

314 4 Results and discussion

315 4.1 Source apportionment of surface PM_{2.5}

316 The simulated spatial distribution of average surface PM_{2.5} levels and the wind
317 vector during the six haze episodes are shown in Fig. 5. In general, two types of patterns
318 were observed. The first pattern corresponded to Ep1, Ep4, and Ep6 and reflected that
319 a highly polluted belt with >200 µg m⁻³ PM_{2.5} extended from the southwest to the
320 northeast along the Taihang mountain range. In the second pattern (Ep2, Ep3, and Ep5),
321 the PM_{2.5} level of 150–200 µg m⁻³ was concentrated in three northern cities (Beijing,
322 Tianjin, and Tangshan). In the other cities, the PM_{2.5} mass concentrations ranged from
323 75 to 115 µg m⁻³, indicating a light pollution level according to the Technical
324 Regulation on Ambient Air Quality Index (on trial).

325 Figure 6 shows the contributions of regional transport and local emissions to
326 average PM_{2.5}, primary aerosol (PA, BC and primary PM_{2.5}), and SIA levels in different
327 cities during the study period. The contribution of local emissions was more than that
328 of regional transport to the PM_{2.5} mass concentration in all cities, except Heng Shui,
329 Cangzhou, Langfang, and Qinhuangdao; the magnitude of local emission contributions
330 was 49%–80%. The principle reason for this was the accumulation of local PA
331 emissions. In most cities, 64%–93% of PA originated from local emissions (Fig. 6c). In
332 contrast to PA, the SIA contribution was dominated by regional transport of emissions
333 in other cities (50%–87%). Even the emissions of cities outside the city cluster (e.g.,
334 Henan, Shanxi and Shandong) were transported to the megacity cluster, travelling 500–
335 1,000 km. In Beijing, the local contribution to total PM_{2.5} and PA was 74% and 94%,
336 respectively, whereas regional transport from other cities was the major source of SIA,
337 contributing 51%. The difference in source apportionment between PA and SIA was
338 related to the mechanisms of PA and SIA formation. Regarding PA, the inversion layer



339 and weak winds during stable weather conditions prevented PA transport and resulted
340 in local-scale accumulation of PA emissions. SIA mostly originated from the chemical
341 conversion of its gaseous precursors (e.g., SO₂, NO₂, and NH₃). The regional transport
342 provided sufficient time (1–3 days) and aerosol surface for this chemical transformation
343 (Li et al., 2015; Li et al., 2017). This also indicates that regional controls would be the
344 most efficient way to decreasing the SIA concentration in this megacity cluster. Our
345 results agree favorably with the observed impact of regional emission controls in Asia-
346 Pacific Economic Cooperation China 2014. During this gathering, the SIA
347 concentration in Beijing decreased to a greater degree than the PA concentration
348 because of regional controls (Sun et al., 2016).

349 The source apportionment in haze episodes in Beijing is illustrated in Fig. 7.
350 Regional transport contributed 14%–31% to the surface PM_{2.5} mass concentration
351 during the six episodes. The highest contribution of regional transport occurred in Ep1
352 and Ep5 (29% and 31% of the total PM_{2.5}, respectively). In Ep1 and Ep5, the
353 contribution of the SIA originating from regional transport reached 53% and 63%,
354 respectively. Interestingly, the regionally transported SIA had different source regions
355 in Ep1 and Ep5. In Ep5, SX, WHB, and NHB were the dominant source regions,
356 whereas the source regions for Ep1 were more diverse. This indicates the complexity
357 of regional transport in this megacity cluster. Compared with the episodes in November
358 2015, the effects of regional transport of PM_{2.5} and SIA mass concentrations were
359 weaker in this study, which may be related to the weather system and emission controls
360 in 2016 (Li et al., 2017). Therefore, more studies on regional transport should be
361 conducted to further understand regional haze formation mechanisms. In other episodes
362 (Ep2, Ep3, Ep4, and Ep6), regional transport of surface PM_{2.5}, PA, OM, and SIA mass
363 concentrations were in the range 14%–23%, 3%–12%, 3%–14%, and 30%–51%,
364 respectively. Local emissions during the episodes were more dominant than the
365 monthly averages.

366 Figure 8 presents the relative contribution of regionally transported SIA under
367 different levels of pollution in Beijing. The source regions varied considerably under



different pollution levels. Under clean conditions (when $SIA < 50 \mu\text{g m}^{-3}$), NHB and SX were the main source regions, contributing up to 30% and 19%, respectively. With the increase of SIA concentrations, WHB, SD, and EHB became the main source regions, contributing 27%, 15%, and 13%, respectively, which is consistent with transport along the southwest and southeast corridors of BTH. Under heavy pollution, pollutants from HN and farther regions were blown to Beijing, resulting in a remarkably higher contribution of HN. This indicates that wider regional emission control is necessary to reduce severe pollution.

4.2 Impact of regional transport of sulfate and its precursors on Beijing

Quantifying the impact of regional transport of sulfate and its precursors is a crucial task. Sun et al. (2014) considered sulfate formed outside Beijing as regionally transported sulfate, and they estimated that its contribution reached 67% during winter haze episodes. By tagging emissions regions of precursors in models and ignoring where secondary aerosols were formed, Li et al. (2017) and Timmermans et al. (2017) estimated the contribution of transport to be 40%–50%. These estimated contributions of regional transport are different in physical meaning, which may confuse policymakers. In this study, we divided the sulfate mass concentration in Beijing into four parts, LC, LTC, RLC, and RTC as described in Sect. 2.1. The regional transport defined by Sun et al. (2014) was $LTC + RLC + RTC$, whereas in the studies by Li et al. (2017) and Timmermans et al. (2017), it was $RLC + RTC$. In this study, we employed $RLC + RTC$ as representing regional transport.

Figure 9a shows the contributions of LC, LTC, RLC, and RTC to the daily average sulfate concentration in Beijing during the study period. RTC and LC were the dominant sources of sulfate, contributing 71%–89% in total. The contributions of RTC ranged from 29% in Ep6 to 59% in Ep2, and contributions of LC were 30%–42%. RTC dominated the regional transport over the whole period, which indicates that chemical conversions in the transport pathway of SO_2 were critical to haze formation. Notably,



the LTC contribution was comparable with that of LC in Ep3, Ep4, and Ep6. This suggests that the SO₂ emitted in Beijing was blown away and formed sulfate outside of Beijing. These formed sulfates may have been blown back to Beijing under certain weather conditions and were previously considered regional transport. The contribution of LTC also largely explains the difference in estimated regional transport contributions between Sun et al. (2014) and Li et al. (2017). In the present study, LTC + RLC + RTC accounted for 58%–70% of the sulfate concentration in the six episodes, which is relatively similar to the estimation (75%) of Sun et al. (2014), which was based on the observed hourly rate of increase of local sulfate concentration.

In the initial and subsequent pollution stages, LC, LTC, and RTC showed different patterns in Beijing. In Ep1, local contributions dominated before the sulfate concentration increased rapidly (November 15 and 16). In particular, sulfate blown back to Beijing from its local emissions (LTC) made a larger contribution (35%) than RTC (25%). In the rapid rising phase of sulfate (November 17 and 18), contribution of RTC increased from 25% to 47%. LC was also significant and increased considerably from 37% to 41%. These two parts (LC and RTC) explained the rapid formation of sulfate in Beijing. This suggests that the joint control of local and regional SO₂ emissions is essential for preventing the rapid formation of haze in this region, which is receiving considerable attention and eliciting widespread interest among the researchers and policymakers (Sun et al., 2014; Ma et al., 2017; Li et al., 2017). This feature is also reflected in Fig. 9b. Under clear conditions (sulfate < 20 µg m⁻³), the local contributions (LC and LTC) were positively correlated with the sulfate mass concentration. In total, they contributed 40%–60% of the sulfate mass concentration. The ratio of LC to LTC was approximately 2:1. Under moderate sulfate levels (20 µg m⁻³ < sulfate < 35 µg m⁻³), the local contribution was lower—particularly the LTC—leading to a ratio of LC to LTC of approximately 8. Sulfate formed in the regional transport pathway (RTC) significantly increased from 40 to 65%. Under heavy pollution levels (> 35 µg m⁻³), the LC was up to at 50% due to extremely stable boundary layers. Our results are consistent with those of Ma et al. (2017), in which



regional transport and local heterogeneous chemistry were qualitatively discovered to make high contributions to initial and subsequent pollution stages.

4.3 Evolution of aerosol properties in Beijing during haze episodes

Aerosol properties such as the particle size and aging degree can change dramatically on haze days because of fresh emissions, subsequent chemical conversions, and regional transport, which strongly affect regional radiation and climate (Cappa et al., 2012). As illustrated in Fig. 4b, the GMD of aerosols in Beijing increased remarkably to approximately 120 nm during the six haze episodes, compared with the GMD of 50 nm under clean conditions. Two stages were identified: an initial rising stage and a sustained increase stage. In the initial stage, the GMD of aerosols increased by 50–60 nm for several hours, and the GMD then remained at 100–120 nm for several days in the subsequent elevated pollution stage. This GMD increase during the initial stage was mainly caused by the increase of accumulation-mode particles with diameters of 100–1,000 nm and Aitken-mode particles (Fig. 10). Under clean conditions ($\text{SIA} < 50 \mu\text{g m}^{-3}$), the average contributions of the three modes (nucleation, Aitken, and accumulation modes) to the number concentration were comparable, although the number of nucleation-mode particles decreased with SIA concentration. Under light-moderate pollution conditions ($50 < \text{SIA} < 150 \mu\text{g m}^{-3}$), the proportion of accumulation-mode particles significantly increased from 35% to 60%, whereas the proportion of Aitken-mode particles slowly decreased. As discussed in previous sections, regional transport played a dominant role during the initial stage. This indicates that condensation, coagulation, and chemical transformation in the transport pathway increased the number of particles with a diameter range of 100–1,000 nm. Finally, the contributions of Aitken-mode and accumulation-mode particles remained stable under the heavy-pollution conditions ($\text{SIA} > 150 \mu\text{g m}^{-3}$).

Aging processes play a critical role in the growth of particles during haze episodes. According to observations, a significant coating of secondary components on BC was



453 found in the study period (Wang et al., 2018). Figure 11 presents a time series of the
454 simulated R_{BC} , which is a favorable indicator of the aging degree (Oshima et al., 2009;
455 Collier et al., 2018). Higher R_{BC} indicates that BC had undergone a greater degree of
456 aging. In this study, the simulated R_{BC} was 2–10, with an average value of 4.5. This
457 value is higher than that for fresh traffic source particles (Liu et al., 2017). Under
458 pollution conditions, R_{BC} was higher than that under clean conditions, with an average
459 value of 5.0. R_{BC} in Beijing even exceeded 10.0 in some extremely severe pollution
460 events, which is close to observations of remote sites (Wang et al., 2017; Massoli et al.,
461 2015) and aged particles (Cappa et al., 2012). Urban aerosols usually have a lower R_{BC}
462 because of fresh emissions and high R_{BC} in this study indicates that Beijing aerosol
463 particles were more aged during the haze episodes. On clean days, R_{BC} ranged from 2
464 to 5, with an average of 2.8. This is similar to the R_{BC} of vehicle emissions (<3) (Liu et
465 al, 2017). Vehicle emissions contributed 70% of BC in downtown Beijing in 2016 after
466 strict controls on coal burning had been implemented (Kebin He, personal
467 communication).

468 Figure 12 shows the evolution of R_{BC} , the size distribution of number
469 concentrations, and the GMD along the transport pathway from the source region to
470 Beijing during the six haze episodes. The transport pathway was calculated using the
471 HYSPLIT model. The figure clearly shows that the aerosol properties changed
472 considerably along the transport pathway. In Ep1, the GMD of aerosols was only 97
473 nm at the initial site of the 24 h back trajectories (T_{-24}). At a larger transport distance,
474 the diameters of aerosol particles were markedly increased to 128 nm in the middle (T_{-12})
475 and 134 nm at the final site (T_0) of the back trajectory. R_{BC} increased from 3.6 at T_{-24}
476 to 8.7 at Beijing (T_0) because of BC being coated during the transport. This indicates
477 that BC underwent considerable aging and increased in size while moving along the
478 transport pathway; this would affect radiation and climate change (Cappa et al., 2012).
479 Similar characteristics were discovered for Ep3–6. In Ep3, Ep4, Ep5, and Ep6, the
480 GMD in Beijing (T_0) was 126, 117, 124, and 116 nm, respectively, compared with 96,
481 95, 99, and 111 nm in the middle point of transport (T_{-12}). R_{BC} also increased to 4.6–7.6.



482 An exception was Ep2, in which the GMD (106 nm) and R_{BC} (3.8) at the final ending
483 site (Beijing, T_0) were lower than those 6 h previously (T_{-6}). Regional transport
484 contributed 95% of BC at T_{-6} , whereas local emissions accounted for 87% of BC at T_0 .
485 The number concentration was smaller at T_{-6} than that at T_0 . Therefore, we conclude
486 that regional transport of aged aerosols led to a high GMD at T_{-6} , and that the addition
487 of locally emitted fresh air caused a high number concentration but low GMD at T_0 . In
488 clean areas, such as at T_{-24} in Ep3 and Ep5, R_{BC} was higher than 10 and the GMD was
489 considerably smaller.

490 **4.4 Impact of heterogeneous chemistry on sulfate mass** 491 **concentration**

492 Current models generally account for a part of the observed SO_4^{2-} concentrations
493 in China (Wang et al., 2014). Heterogeneous chemistry on aerosol surfaces under high
494 relative humidity has been considered a potential missing source of sulfate formation
495 (Cheng et al., 2016; Zheng et al., 2015; Li et al., 2017; Tang et al., 2016). Li et al. (2018)
496 developed a simple parameterization of heterogeneous chemistry and discovered that
497 SO_2 uptake on aerosols partly closed the gap between simulation and observation. In
498 their study, uptake coefficients were dependent on the aerosol core and shell species,
499 shell thickness, and amount of aerosol liquid water. Zheng et al. (2013) and Yang et al.
500 (2014) measured local source profiles, and they reported that primary sulfate from
501 industry and power plants accounted for a large fraction of PA.

502 In this study, we examined the contributions of gas ($SO_2 + OH$) and aqueous
503 chemistry, heterogeneous chemistry, and primary sulfate emissions to the sulfate mass
504 concentration in Beijing (Fig. 13). In Ep1, under high relative humidity, the contribution
505 of heterogeneous chemistry was 33%. Primary emissions exerted an effect mostly under
506 light to moderate pollution levels (sulfate $< 20 \mu g m^{-3}$), whereas heterogeneous
507 chemistry played the largest role under high pollution levels (sulfate $> 30 \mu g m^{-3}$). The
508 contributions of gas and aqueous chemistry were largely consistent under all pollution



509 conditions (~30%). This indicates that high relative humidity and aerosol loading
510 accelerated the SO₂ chemical transformation. Interestingly, the contribution of
511 heterogeneous chemistry was markedly higher when the sulfate mass concentration
512 exceeded the threshold of 20 µg m⁻³. Under high relative humidity and mass
513 concentration conditions, a higher aerosol surface area resulting from hygroscopic
514 growth provided a favorable media for heterogeneous reactions (Tie et al., 2017). The
515 aforementioned threshold is relatively similar to that during the haze episodes in the
516 winter of 2013 (Li et al, 2018). For policymakers, implementing measures to prevent
517 the sulfate concentration from exceeding this threshold is essential. Such measures
518 would be effective for avoiding extremely high sulfate levels. In other episodes,
519 heterogeneous chemistry was depressed because of the low relative humidity (<70%).
520 Gas and aqueous chemistry and primary emissions contributed 35%–40% and 58%–
521 61%, respectively. It should be noted that failure of the model to simulate mineral dust
522 led to underestimation of the sulfate level in Ep2. The interaction between SO₂ and
523 alkaline dust can contribute considerably to the sulfate concentration.

524 5 Conclusions

525 The contributions of regional transport to haze episodes over a megacity cluster
526 centered on Beijing have been under debate in recent decades. Investigating the
527 evolution of aerosol properties along the transport pathway may provide more
528 information on how researchers can improve the accuracy of regional transport and
529 chemistry impact assessments. To address one of the aims of the APHH 2016 winter
530 campaign, we employed a Eulerian chemical transport model (NAQPMS) and a
531 Lagrangian trajectory model (HYSPLIT) to assess the evolution of aerosols—in terms
532 of the number concentration, size distribution, and aging degree—in Beijing during six
533 haze episodes between November 15 and December 15, 2016. The transport of sulfate
534 and its precursors was also quantitatively investigated.

535 The results demonstrated that regional transport contributed 14%–31% to the
536 surface PM_{2.5} mass concentration in Beijing during the six episodes, with a monthly



average contribution of 26%. Regarding aerosol components, 30%–62% of the SIA in Beijing were regionally transported, whereas few PAs (<10%) were contributed from emissions in other regions. Source regions differed between episodes. During high-pollution periods, WHB, SD, and EHB were the main source regions of SIA regionally transported to Beijing, whereas NHB and SX made greater contributions under clean and light pollution conditions. This indicates the complexity of regional transport in this megacity cluster.

The chemical transformation of SO₂ along the transport pathway from source regions except Beijing to Beijing (RTC) was the major form of SO₄²⁻ regional transport and was more critical than the transport of sulfate formed in source regions except Beijing (RTC). Compared with sulfate that was chemically transformed from Beijing-emitted SO₂ and then blown back to Beijing (LTC), contribution of sulfate produced in Beijing from Beijing-emitted SO₂ (LC) was generally greater. However, RTC markedly increased in some episodes, and this explains the rapid formation of sulfate in Beijing. This suggests that the joint control of local and regional SO₂ emissions is essential for reducing the rapid formation of haze in this region.

Aerosols became considerably aged during transport in haze episodes, which altered R_{BC} and the size distribution of number concentrations. During haze episodes, the GMD increased from less than 100 nm at the initial site to approximately 120 nm at the final site (Beijing), and R_{BC} increased from 2–4 to 4–8. The number of accumulation-mode particles with a diameter range of 100–1,000 nm increased considerably more than the number of particles of different modes. R_{BC} in Beijing during the episodes was higher than that of fresh particles (<1.5), which indicates that BC in Beijing was more aged and thus more likely to affect radiation and climate.

Contributions from different pathways to sulfate in Beijing were also examined. In episodes with high humidity (Ep1), the average contributions of gas and aqueous chemistry, heterogeneous chemistry, and primary sulfate were comparable. Primary emissions mostly had an effect under light to moderate pollution levels, whereas



heterogeneous chemistry played the most crucial role under high pollution levels. In other episodes (Ep2, Ep3, Ep4, Ep5, and Ep6), gas and aqueous chemistry and primary emissions contributed 35%–40% and 58%–61%, respectively.

Acknowledgements:

This work was supported by the Natural Science Foundation of China (41571130034; 91544227; 91744203; 41225019; 41705108) and the Chinese Ministry of Science and Technology (2018YFC0213205 and 2017YFC0212402).

References

- Anderson, H. R., Atkinson, R., Balbus, J., Brauer, M., Chapman, R., Chowdhury, Z.: Outdoor Air Pollution and Health in the Developing Countries of Asia: A Comprehensive Review, Special Report 18, Health Effects Institute, Boston, Massachusetts, 2010.
- Boylan, J. W., & Russell, A. G.: PM and light extinction model performance metrics, goals, and criteria for three-dimensional air quality models, *Atmospheric Environment*, 40(26), 4946–4959, <https://doi.org/10.1016/j.atmosenv.2005.09.087>, 2006.
- Cao J.: PM_{2.5} and environment. Science Press, 2014.
- Cappa, C. D., Onasch, T. B., Massoli, P., Worsnop, D. R., Bates, T. S., Cross, E. S., ... Zaveri, R. A.: Radiative Absorption Enhancements Due to the Mixing State of Atmospheric Black Carbon, *Science*, 337(6098), 1078–1081, <https://doi.org/10.1126/science.1223447>, 2012.
- Chen, X., Li, X., Yuan, X., Zeng, G., Liang, J., Li, X., ... Chen, G.: Effects of human activities and climate change on the reduction of visibility in Beijing over the past 36years, *Environ Int*, 116, 92–100, <https://doi.org/10.1016/j.envint.2018.04.009>, 2018.
- Chen, X., Wang, Z., Li, J., & Yu, F.: Development of a regional chemical transport model with size-resolved aerosol microphysics and its application on aerosol number concentration simulation over china, *Scientific Online Letters on the Atmosphere Sola*, 10, 83–87, <https://doi.org/10.2151/sola.2014-017>, 2014.
- Chen, X., Wang, Z., Yu, F., Pan, X., Li, J., & Ge, B., et al.: Estimation of atmospheric aging time of black carbon particles in the polluted atmosphere over central-eastern china using microphysical process analysis in regional chemical transport model. *Atmospheric Environment*, 163, 44–56, <https://doi.org/10.1016/j.atmosenv.2017.05.016>, 2017.
- Cheng, Y., Zheng, G., Wei, C., Mu, Q., Zheng, B., & Wang, Z., et al: Reactive nitrogen chemistry in aerosol water as a source of sulfate during haze events in china, *Science Advances*, 2(12), <https://doi.org/10.1126/sciadv.1601530>, 2016.
- Collier, S., Williams, L. R., Onasch, T. B., Cappa, C. D., Zhang, X., & Russell, L. M., et al: Influence



- 598 of emissions and aqueous processing on particles containing black carbon in a polluted urban
599 environment: insights from a soot particle-aerosol mass spectrometer, *Journal of Geophysical*
600 *Research Atmospheres*, 123(12), 6648-6666, <https://doi.org/10.1002/2017jd027851>, 2018.
- 601 Draxler, R. R., & Hess, G. D: An overview of the HYSPLIT 4 modeling system for trajectories,
602 dispersion, and deposition, *Australian Meteorological Magazine*, 47(4), 295-308, 1998.
- 603 Du, W., Zhao, J., Wang, Y., Zhang, Y., Wang, Q., & Xu, W., et al: Simultaneous measurements of
604 particle number size distributions at ground level and 260 m on a meteorological tower in urban
605 Beijing, china, *Atmospheric Chemistry & Physics*, 17(11), 6797-6811,
606 <https://doi.org/10.5194/acp-17-6797-2017>, 2017.
- 607 Han, B., Zhang, R., Yang, W., Bai, Z., Ma, Z., & Zhang, W: Heavy haze episodes in Beijing during
608 January 2013: inorganic ion chemistry and source analysis using highly time-resolved
609 measurements from an urban site, *Science of the Total Environment*, 544, 319-329,
610 <https://doi.org/10.1016/j.scitotenv.2015.10.053>, 2016.
- 611 Huang, R. J., Zhang, Y., Bozzetti, C., Ho, K. F., Cao, J. J., Han, Y., . . . Prevot, A. S: High secondary
612 aerosol contribution to particulate pollution during haze events in China, *Nature*, 514(7521),
613 218-222, <https://doi.org/10.1038/nature13774>, 2014.
- 614 Hyslop, N. P.: Impaired visibility: the air pollution people see, *Atmospheric Environment*, 43(1),
615 182-195, <https://doi.org/10.1016/j.atmosenv.2008.09.067>, 2009.
- 616 Lee, A. K. Y., Chen, C. L., Liu, J., Price, D. J., Betha, R., Russell, L. M., Zhang, X., and Cappa, C.
617 D.: Formation of secondary organic aerosol coating on black carbon particles near vehicular
618 emissions, *Atmos. Chem. Phys.*, 17(24), 15055-15067, [https://doi.org/10.5194/acp-17-15055-](https://doi.org/10.5194/acp-17-15055-2017)
619 [2017](https://doi.org/10.5194/acp-17-15055-2017), 2017.
- 620 Li, G., Bei, N., Cao, J., Huang, R., Wu, J., & Feng, T., et al.: A possible pathway for rapid growth
621 of sulfate during haze days in china, *Atmospheric Chemistry & Physics*, 17(5), 3301-3316,
622 <https://doi.org/10.5194/acp-17-3301-2017>, 2017.
- 623 Li, J., Chen, X., Wang, Z., Du, H., Yang, W., & Sun, Y., et al.: Radiative and heterogeneous chemical
624 effects of aerosols on ozone and inorganic aerosols over east Asia, *Science of the Total*
625 *Environment*, 622-623, 1327, <https://doi.org/10.1016/j.scitotenv.2017.12.041>, 2018.
- 626 Li, J., Du, H., Wang, Z., Sun, Y., Yang, W., & Li, J., et al.: Rapid formation of a severe regional
627 winter haze episode over a mega-city cluster on the North China Plain, *Environmental*
628 *Pollution*, 223, 605-615, <https://doi.org/10.1016/j.envpol.2017.01.063>, 2017.
- 629 Li, J., Han, Z.: A modeling study of severe winter haze events in Beijing and its neighboring regions,
630 *Atmospheric Research*, 170, 87-97, <https://doi.org/10.1016/j.atmosres.2015.11.009>, 2016.
- 631 Li, J., Wang, Z., Huang, H., Min, H. U., Meng, F., & Sun, Y., et al.: Assessing the effects of trans-
632 boundary aerosol transport between various city clusters on regional haze episodes in spring
633 over east china, *Tellus*, 65(1), 60-73, <https://doi.org/10.3402/tellusb.v65i0.20052>, 2013.
- 634 Li, J., Yang, W., Wang, Z., Chen, H., Hu, B., & Li, J., et al.: A modeling study of source–receptor
635 relationships in atmospheric particulate matter over northeast Asia. *Atmospheric Environment*,



- 636 91(7), 40-51, <https://doi.org/10.1016/j.atmosenv.2014.03.027>, 2014.
- 637 Li, J., Wang, Z.F., Zhuang, G., Luo, G., Sun, Y., Wang, Q.: Mixing of Asian mineral dust with
638 anthropogenic pollutants over East Asia: a model cast study of a super-dust storm in March
639 2010. Atmos. Chem. Phys. 12 (16), 7591-7607. <https://dx.doi.org/10.5194/acp-12-7591-2012>,
640 2012.
- 641 Li, P., Yan, R., Yu, S., Wang, S., Liu, W., & Bao, H.: Reinstate regional transport of PM_{2.5} as a major
642 cause of severe haze in Beijing, Proc Natl Acad Sci U S A, 112(21), E2739-2740,
643 <https://doi.org/10.1073/pnas.1502596112>, 2015.
- 644 Liu, D., Whitehead, J., Alfarra, M. R., Reyes-villegas, E., Spracklen, D. V., & Reddington, C. L., et
645 al.: Black-carbon absorption enhancement in the atmosphere determined by particle mixing
646 state, Nature Geoscience, 10(3), 184-188, <https://doi.org/10.1038/ngeo2901>, 2017.
- 647 Liu, X., Zhang, Y., Jung, J., Gu, J., Li, Y., & Guo, S., et al.: Research on the hygroscopic properties
648 of aerosols by measurement and modeling during CAREBeijing-2006, Journal of Geophysical
649 Research Atmospheres, 114(16), 4723-4734, <https://doi.org/10.1029/2008jd010805>, 2009.
- 650 Ma, Q., Wu, Y., Zhang, D., Wang, X., Xia, Y., Liu, X., . . . Zhang, R.: Roles of regional transport
651 and heterogeneous reactions in the PM_{2.5} increase during winter haze episodes in Beijing, Sci
652 Total Environ, 599-600, 246-253, <https://doi.org/10.1016/j.scitotenv.2017.04.193>, 2017.
- 653 Ma, X., & Yu, F.: Seasonal variability of aerosol vertical profiles over east us and west Europe:
654 GEOS-Chem/APM simulation and comparison with CALIPSO observations, Atmospheric
655 Research, 140-141(31), 28-37, <https://doi.org/10.1016/j.atmosres.2014.01.001>, 2014.
- 656 Ma, Z., Liang YP, Zhang J.: PM_{2.5} profiles of typical sources in Beijing, Acta Science
657 Circumstantiae, 35(12), 4043-4052, <https://doi.org/10.13671/j.hjkxxb.2015.0584>, 2015.
- 658 Massoli, P., Onasch, T. B., Cappa, C. D., Nuamaan, I., Hakala, J., & Hayden, K., et al.:
659 Characterization of black carbon containing particles from soot particle aerosol mass
660 spectrometer measurements on the R/V Atlantis during CalNex 2010, Journal of Geophysical
661 Research Atmospheres, 120(6), 2575-2593, <https://doi.org/10.1002/2014jd022834>, 2015.
- 662 Nenes, A., Pandis, S.N., Pilinis, C.: ISORROPIA: A new thermodynamic equilibrium model for
663 multiphase multicomponent inorganic aerosols, Aquat. Geochem. 4(1), 123-152.
664 <https://dx.doi.org/10.1023/A:1009604003981>, 1998.
- 665 Oshima, N., Koike, M., Zhang, Y., Kondo, Y., Moteki, N., & Takegawa, N., et al.: Aging of black
666 carbon in outflow from anthropogenic sources using a mixing state resolved model: model
667 development and evaluation, Journal of Geophysical Research Atmospheres, 114(D6),
668 <https://doi.org/10.1029/2008jd010680>, 2009.
- 669 Pan, X., Ge, B., Wang Z., Tian, Y., et al.: Synergistic effect of water-soluble species and relative
670 humidity on morphological changes of aerosol particles in Beijing mega-city during severe
671 pollution episodes, Atmos. Chem. Phys. Discuss, 1-24, <https://doi.org/10.5194/acp-2018-623>,
672 2018.
- 673 Peng J, Hu M, Guo S, et al.: Markedly enhanced absorption and direct radiative forcing of black



- 674 carbon under polluted urban environments, *Proc Natl Acad Sci USA*, 113(16), 4266-4271,
675 <https://doi.org/10.1073/pnas.1602310113>, 2016.
- 676 Sun, Y., Chen, C., Zhang, Y., Xu, W., Zhou, L., Cheng, X., . . . Wang, Z.: Rapid formation and
677 evolution of an extreme haze episode in Northern China during winter 2015, *Sci Rep*, 6(1),
678 27151. <https://doi.org/10.1038/srep27151>, 2016.
- 679 Sun, Y., Du, W., Wang, Q., Zhang, Q., Chen, C., & Chen, Y., et al. Real-time characterization of
680 aerosol particle composition above the urban canopy in Beijing: insights into the interactions
681 between the atmospheric boundary layer and aerosol chemistry, *Environmental Science &*
682 *Technology*, 49(19), 11340-11347, <https://doi.org/10.1021/acs.est.5b02373>, 2015.
- 683 Sun, Y., Jiang, Q., Wang, Z., Fu, P., Li, J., Yang, T., & Yin, Y.: Investigation of the sources and
684 evolution processes of severe haze pollution in Beijing in January 2013, *Journal of Geophysical*
685 *Research: Atmospheres*, 119(7), 4380-4398, <https://doi.org/10.1002/2014jd021641>, 2014.
- 686 Tang, G., Zhang, J., Zhu, X., Song, T., Münkel, C., Hu, B., et al.: Mixing layer height and its
687 implications for air pollution over Beijing, China, *Atmos. Chem. Phys.*, 16(4), 2459-2475,
688 <https://doi.org/10.5194/acp-16-2459-2016>, 2016.
- 689 Tang, M. J., Larish, W. A., Fang, Y., Gankanda, A., and Grassian, V. H.: Heterogeneous Reactions
690 of Acetic Acid with Oxide Minerals: Effects of Mineralogy and Relative Humidity, *J. Phys.*
691 *Chem. A*, 120(28), 5609-5616, <https://doi.org/10.1021/acs.jpca.6b05395>, 2016.
- 692 Tie, X., Huang, R. J., Cao, J., Zhang, Q., Cheng, Y., Su, H., . . . O'Dowd, C. D.: Severe Pollution in
693 China Amplified by Atmospheric Moisture, *Sci Rep*, 7(1), [https://doi.org/10.1038/s41598-017-](https://doi.org/10.1038/s41598-017-15909-1)
694 [15909-1](https://doi.org/10.1038/s41598-017-15909-1), 2017.
- 695 Timmermans, R., Kranenburg, R., Manders, A., Hendriks, C., Segers, A., & Dammers, E., et al.:
696 Source apportionment of PM_{2.5} across china using LOTOS-EUROS, *Atmospheric*
697 *Environment*, 164, 370-386, <https://doi.org/10.1016/j.atmosenv.2017.06.003>, 2017.
- 698 Wang, J., Liu, D., Ge, X., Wu, Y., Shen, F., Chen, M., . . . Sun, Y.: Characterization of black carbon-
699 containing fine particles in Beijing during wintertime, *Atmospheric Chemistry and Physics*
700 *Discussions*, 1-25, <https://doi.org/10.5194/acp-2018-800>, 2018.
- 701 Wang, J., Zhang, Q., Chen, M. D., Collier, S., Zhou, S., & Ge, X., et al.: First chemical
702 characterization of refractory black carbon aerosols and associated coatings over the Tibetan
703 plateau (4730 m a.s.l), *Environmental Science & Technology*, 51(24), 14072-14082,
704 <https://doi.org/10.1021/acs.est.7b03973>, 2017.
- 705 Wang, S., Zhao, X., Li, X., Wei, W., Hao, J.: Study on fine particle emission characteristics of
706 industrial coal-fired chain furnace. *Environmental Science (Chines)*, 30 (4), 963-968,
707 <https://doi.org/10.3321/j.issn:0250-3301.2009.04.004>, 2009.
- 708 Wang, Y., Zhang, Q., Jiang, J., Zhou, W., Wang, B. Y., He, K. B., . . . Xie, Y. Y.: Enhanced sulfate
709 formation during china's severe winter haze episode in January 2013 missing from current
710 models, *Journal of Geophysical Research Atmospheres*, 119(17), 10425-10440,
711 <https://doi.org/doi:10.1002/2013jd021426>, 2014.



- 712 Wang, Z., Maeda, T., Hayashi, M., Hsiao, L.F., Liu, K.Y.: A nested air quality prediction modeling
713 system for urban and regional scales, application for high-ozone episode in Taiwan, Water, Air,
714 Soil Pollut, 130, 391-396, <https://dx.doi.org/10.1023/A:1013833217916>, 2001.
- 715 Wang, Z., Jie, L., Wang, Z., Yang, W. Y., Tang, X., & Ge, B. Z., et al.: Modeling study of regional
716 severe hazes over mid-eastern China in January 2013 and its implications on pollution
717 prevention and control, Science China Earth Sciences, 57(1), 3-13,
718 <https://dx.doi.org/10.1007/s11430-013-4793-0>, 2014.
- 719 Wiedinmyer, C., Akagi, S. K., Yokelson, R. J., & Emmons, L. K.: The fire inventory from NCAR
720 (FINN) – a high resolution global model to estimate the emissions from open burning,
721 Geoscientific Model Development, 4(3), 625-641, <https://doi.org/10.5194/gmd-4-625-2011>,
722 2011.
- 723 Wu, J. B., Wang, Z., Wang, Q., Li, J., Xu, J., & Chen, H., et al.: Development of an on-line source-
724 tagged model for sulfate, nitrate and ammonium: A modeling study for highly polluted periods
725 in Shanghai, China. Environmental Pollution, 221, 168-179,
726 <https://doi.org/10.1016/j.envpol.2016.11.061>, 2017.
- 727 Yang, H. H.: Filterable and condensable fine particulate emissions from stationary sources, Aerosol
728 & Air Quality Research, 14(7), 2010-2016, <https://doi.org/10.4209/aaqr.2014.08.0078>, 2014.
- 729 Yang, Y., Liu, X., Qu, Y., Wang, J., An, J., & Zhang, Y., et al.: Formation mechanism of continuous
730 extreme haze episodes in the megacity Beijing, China, in January 2013. Atmospheric Research,
731 155, 192-203, <https://doi.org/10.1016/j.atmosres.2014.11.023>, 2015.
- 732 Yang, Y., Wang, H., Smith, S. J., Easter, R., Ma, P. L., Qian, Y., . . . Rasch, P. J.: Global source
733 attribution of sulfate concentration and direct and indirect radiative forcing, Atmospheric
734 Chemistry and Physics, 17(14), 8903-8922, <https://doi.org/10.5194/acp-17-8903-2017>, 2017a.
- 735 Yang, Y., Wang, H., Smith, S. J., Ma, P.-L., & Rasch, P. J.: Source attribution of black carbon and
736 its direct radiative forcing in China, Atmospheric Chemistry and Physics, 17(6), 4319-4336,
737 <https://doi.org/10.5194/acp-17-4319-2017>, 2017b.
- 738 Ying, Q. Wu, L. Zhang, H.: Local and inter-regional contributions to PM_{2.5} nitrate and sulfate in
739 China, Atmos. Environ., 94, 582-592, <https://doi.org/10.1016/j.atmosenv.2014.05.078>, 2014.
- 740 Yu, F., & Luo, G.: Simulation of particle size distribution with a global aerosol model: contribution
741 of nucleation to aerosol and CCN number concentrations, Atmospheric Chemistry & Physics,
742 9(20), 7691-7710, <https://doi.org/10.5194/acp-9-7691-2009>, 2009.
- 743 Zhao, X. J., Zhao, P. S., Xu, J., Meng, W., Pu, W. W., Dong, F., . . . Shi, Q. F.: Analysis of a winter
744 regional haze event and its formation mechanism in the North China Plain, Atmospheric
745 Chemistry and Physics, 13(11), 5685-5696, <https://doi.org/10.5194/acp-13-5685-2013>, 2013.
- 746 Zheng, B., Zhang, Q., Zhang, Y., He, K. B., Wang, K., Zheng, G. J., . . . Kimoto, T.: Heterogeneous
747 chemistry: a mechanism missing in current models to explain secondary inorganic aerosol
748 formation during the January 2013 haze episode in North China, Atmospheric Chemistry and
749 Physics, 15(4), 2031-2049, <https://doi.org/10.5194/acp-15-2031-2015>, 2015.



750 Zheng M., Zhang Y., Yan C., et al.: Establishment of PM_{2.5} industrial source profile in Shanghai,
751 China Environmental Science, 33(8), 1354-1359, [https://doi.org/10.3969/j.issn.1000-](https://doi.org/10.3969/j.issn.1000-6923.2013.08.002)
752 [6923.2013.08.002](https://doi.org/10.3969/j.issn.1000-6923.2013.08.002), 2013.

753 Zhu, X., Tang, G., Hu, B., Wang, L., Xin, J., & Zhang, J., et al.: Regional pollution and its formation
754 mechanism over north China plain: a case study with ceilometer observations and model
755 simulations, Journal of Geophysical Research Atmospheres, 121(24), 14574-14588,
756 <https://doi.org/10.1002/2016jd025730>, 2016.

757 Zhuang, G. Yi, Z. Duce, R.A. Brown, P.R.: Link between iron and sulphur cycles suggested by
758 detection of Fe(n) in remote marine aerosols, Nature, 355(6360), 537-539,
759 <https://doi.org/10.1038/355537a0>, 1992.

760

761 **Figures**

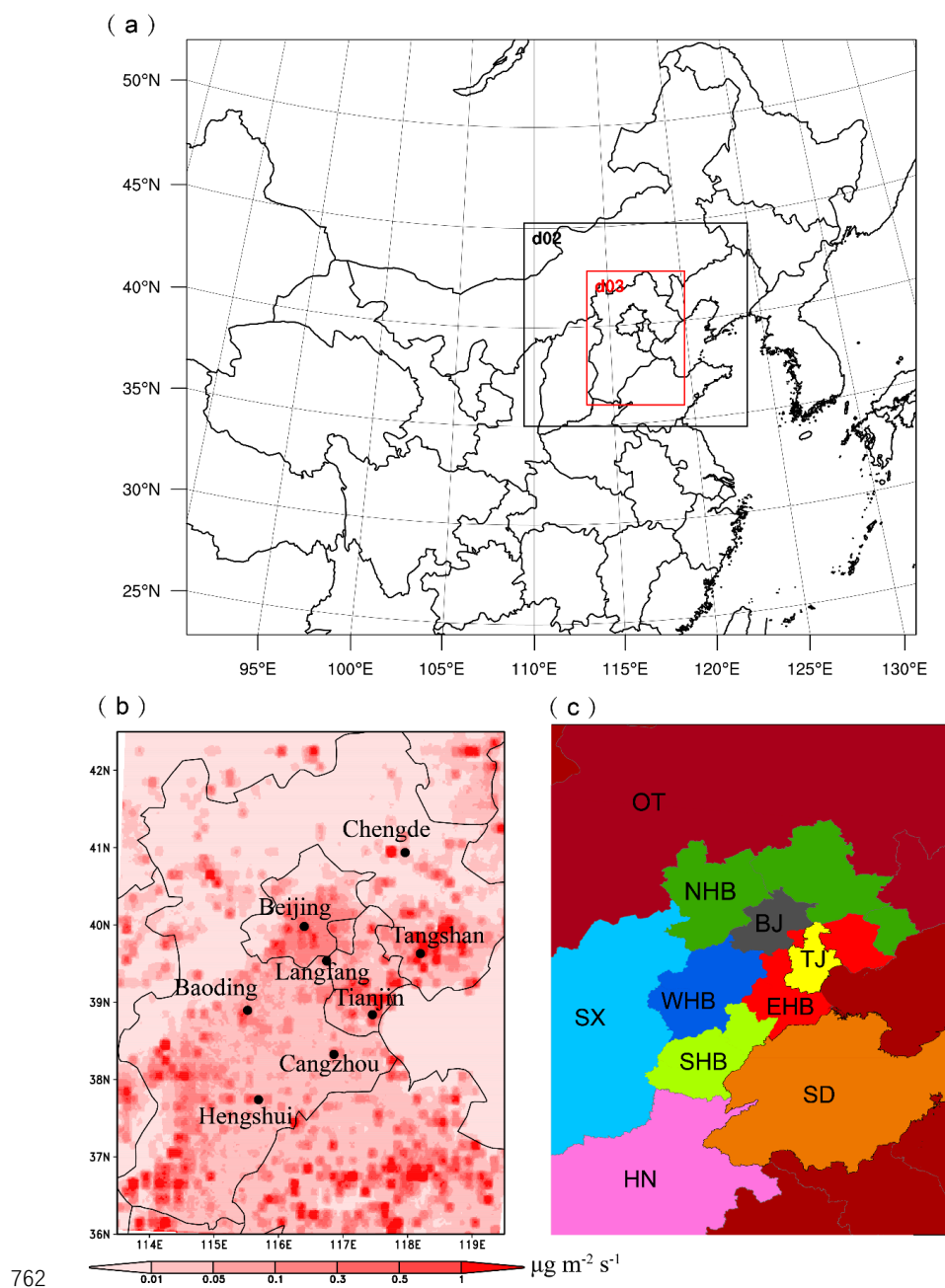
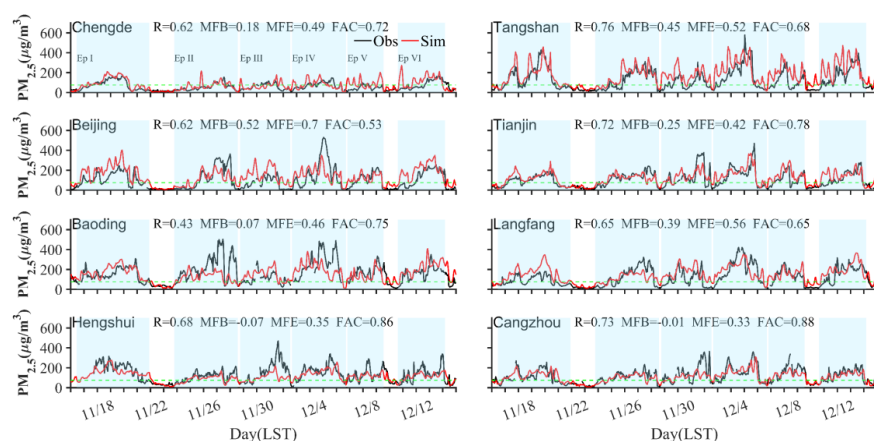


Figure 1. (a) Simulation domains. (b) Primary PM_{2.5} emission rates of the innermost domain and locations of observation sites (black dots). (c) tracer tagging regions which are described in Table 1.

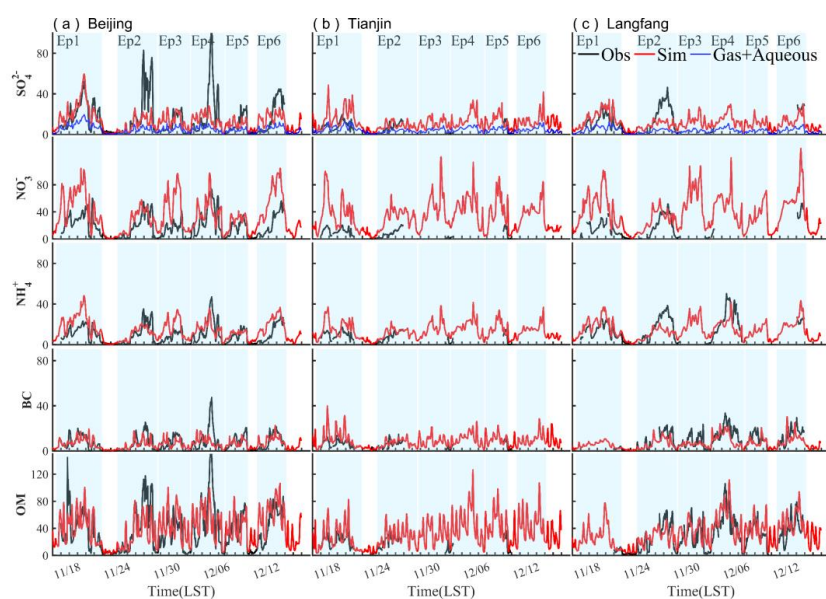


766



767

768 **Figure 2.** Comparison between the simulated and observed hourly concentrations of
 769 $PM_{2.5}$ for different sites. Black lines refer to observation and the red lines are simulation
 770 results; light blue shadows are six episodes identified.

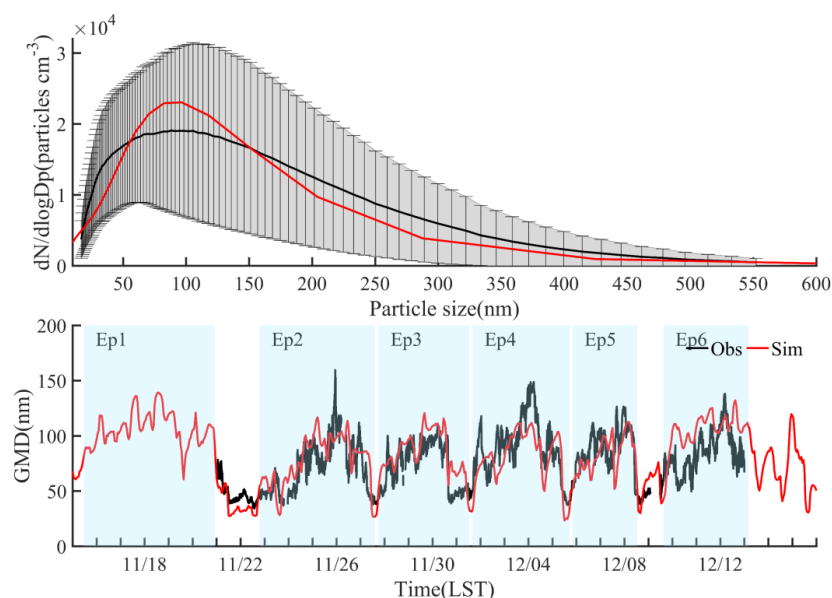


771

772 **Figure 3.** Comparison between the simulated (red) and observed (solid black) hourly
 773 components including sulfate, nitrate, ammonia, black carbon and organic aerosols at
 774 (a) Beijing, (b) Tianjin and (c) Langfang. Blue lines refer to sulfate produced by gas

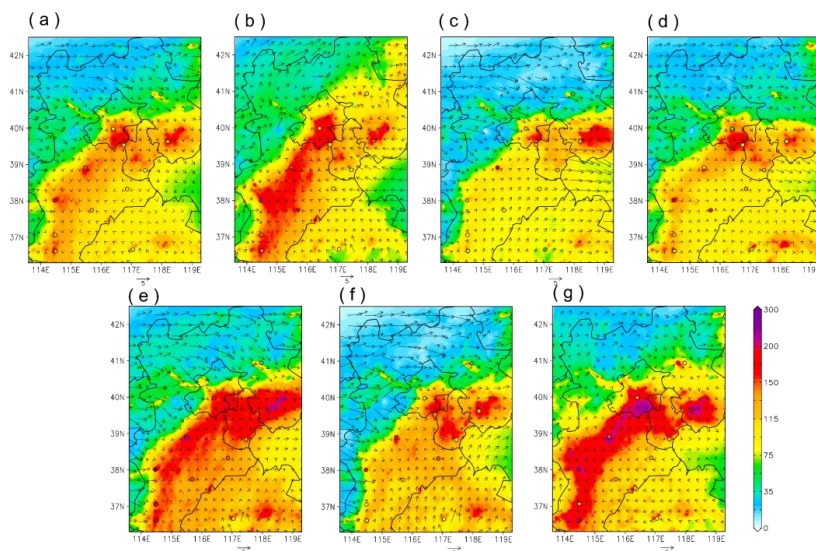


775 and aqueous chemistry reactions.



776

777 **Figure 4.** (a) Particle size distribution in Beijing at ground level. (b) Comparison of
 778 geometric mean diameter (GMD) for particles during range of 16–600nm between
 779 observation and simulation in Beijing. Black solid line and red solid line represent
 780 observation and simulation respectively.

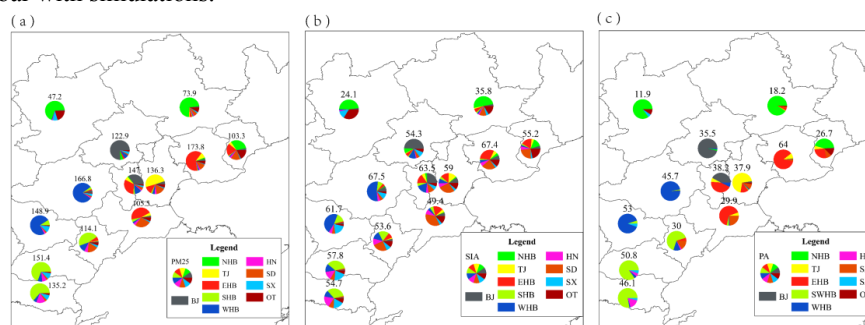


781

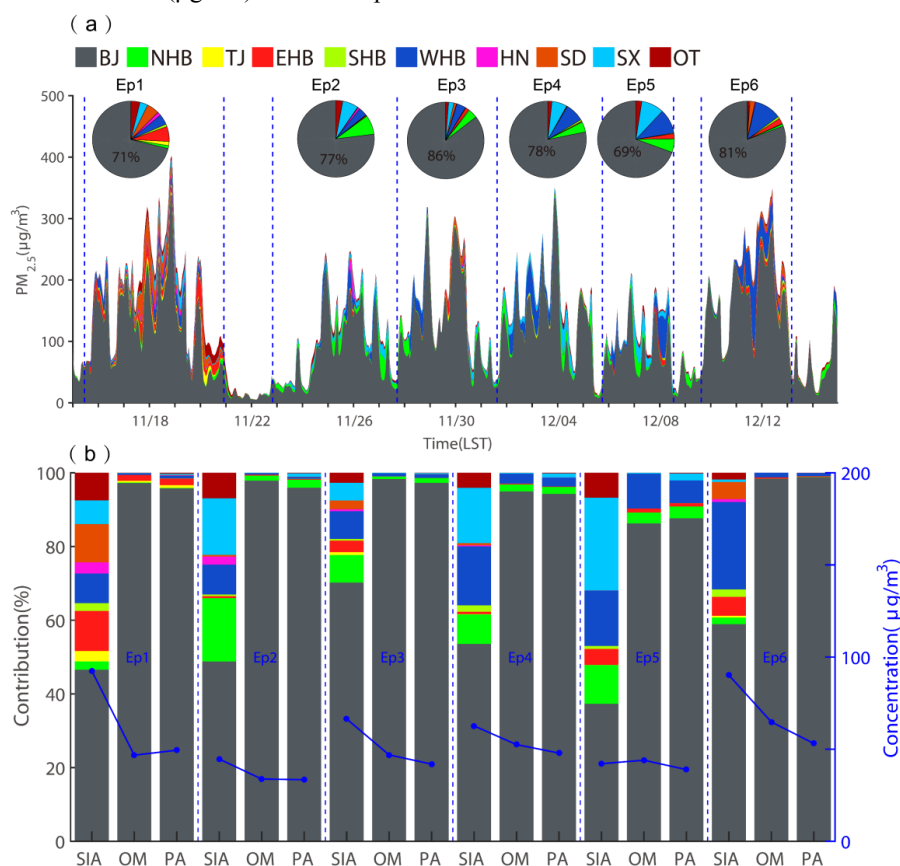
782 **Figure 5.** Spatial distribution of simulated average surface PM_{2.5} (μg m⁻³) and wind (m



783 s^{-1}) over BTH area. (a) average of whole study period, (b)–(g) episode average of
 784 episode1–6 identified before. Solid circles represent observations with the same color
 785 bar with simulations.



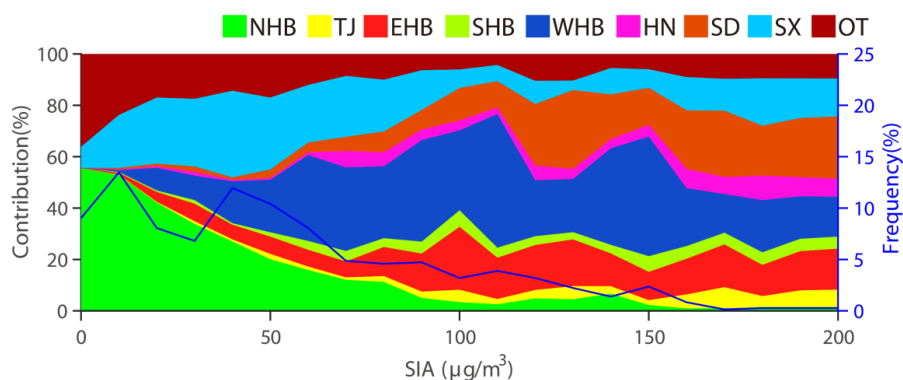
786
 787 **Figure 6.** The contribution of regional transport and local emissions to the average (a)
 788 total $PM_{2.5}$, (b) secondary inorganic aerosols (SIA), (c) primary aerosols (PA, BC and
 789 primary $PM_{2.5}$) over BTH area. The numbers above the pie represent average
 790 concentrations ($\mu g m^{-3}$) of certain species in certain cities.



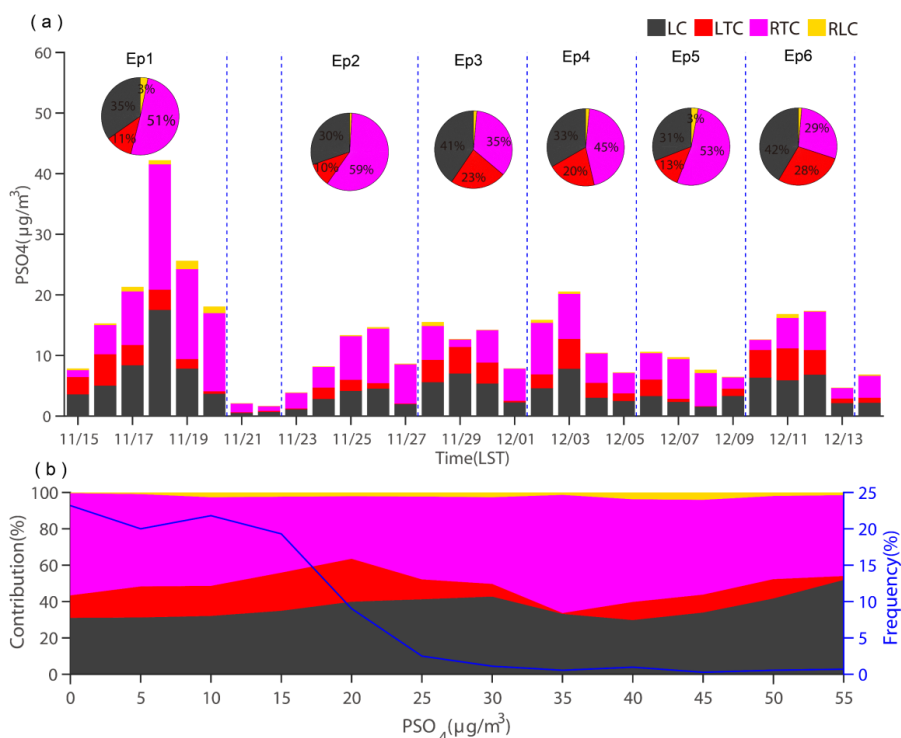
791
 792 **Figure 7.** (a) Source contribution of $PM_{2.5}$ in Beijing and pies represent average status



793 of each episode; (b) Relative contribution of different regions to SIA, OM and PA in
 794 Beijing at the surface layer during each episode (shaded). Concentrations are also
 795 shown (blue line).
 796



797
 798 **Figure 8.** Relative contribution of regionally transported SIA under different levels of
 799 pollution in Beijing during whole study period.



800
 801 **Figure 9.** (a) Regional sources of chemical conversion of secondary sulfate in Beijing.



(b) Variation of region source of chemical conversion of secondary sulfate with hourly surface sulfate concentration level in Beijing for the whole study period. LC means sulfate locally produced from Beijing emitted SO_2 ; LTC refers to sulfate chemically formed in regions except Beijing from the Beijing emitted SO_2 ; RTC is sulfate chemically formed in the transport pathway to Beijing from SO_2 emitted in source regions except Beijing; RLC is sulfate produced in regions except Beijing from locally emitted SO_2 and transported to Beijing.

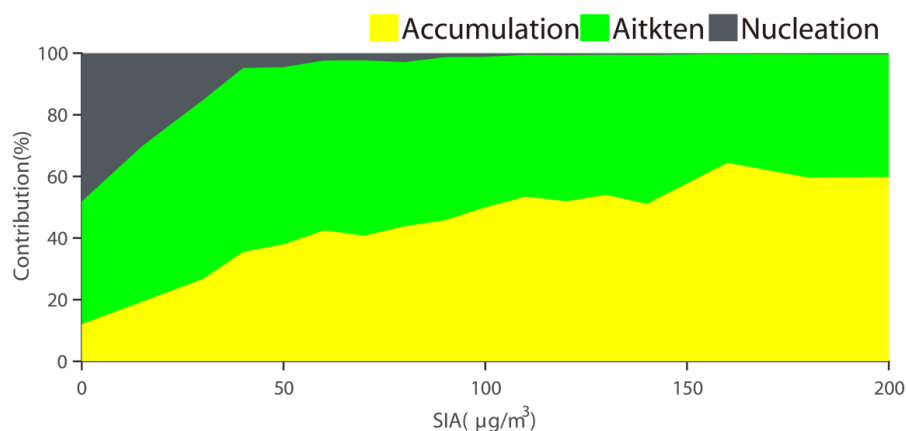
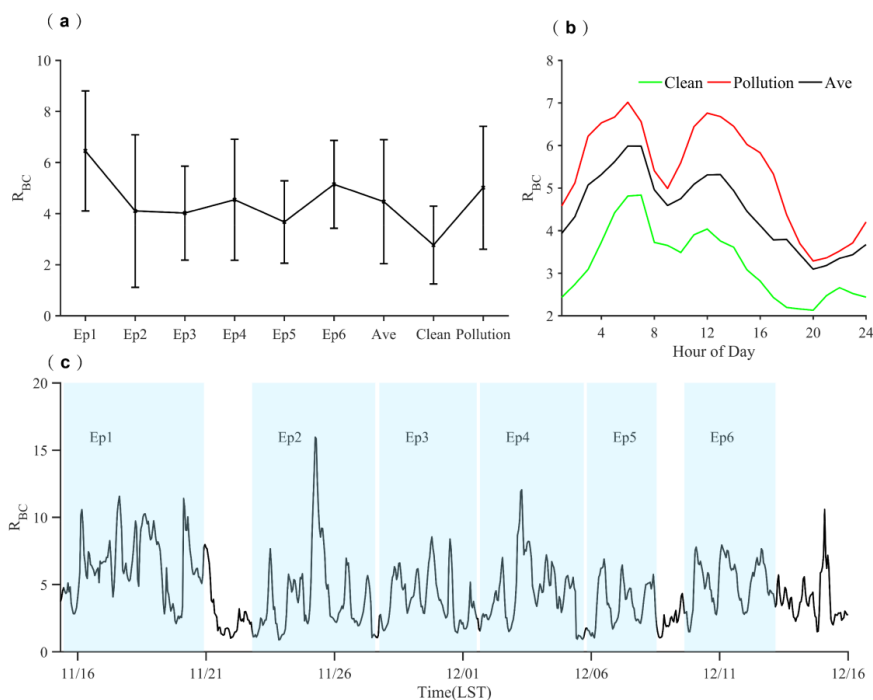


Figure 10. Variation of number concentration fraction of particles with SIA in Beijing during whole study period.



813
 814 **Figure 11.** (a) average and standard variation of massing ratio of coating to BC (R_{BC})
 815 during different episodes and pollution levels, (b) diurnal cycles of R_{BC} under different
 816 pollution levels, (c) temporal variation of R_{BC} during study period.

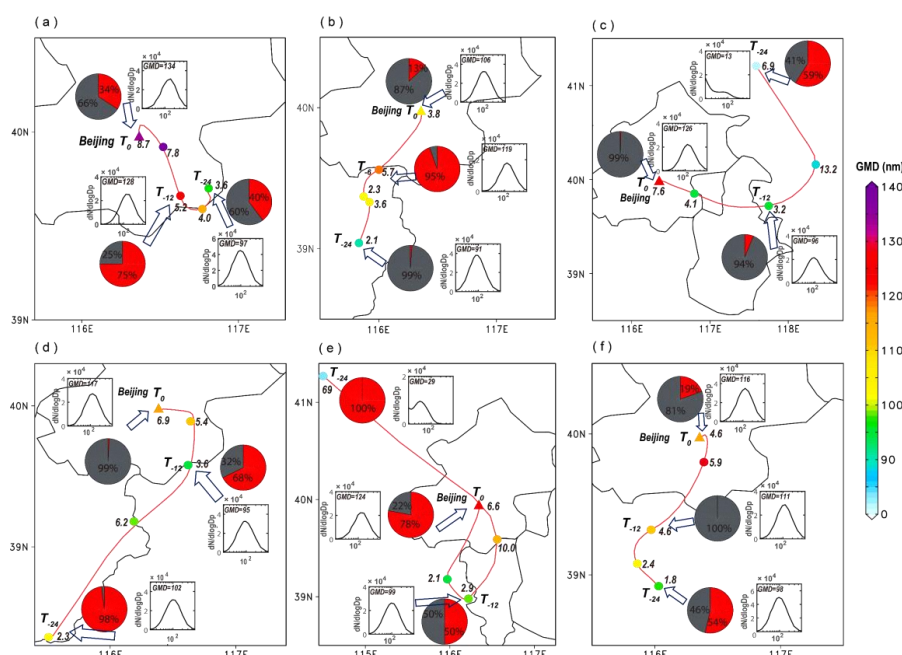


Figure 12. 24 h back trajectories for air mass at the altitude of 100 m and aerosol properties along each trajectory. Panel a–f refers to episode 1–6 at 21:00 on November 18, 22:00 on November 25, 16:00 on November 29, 22:00 on December 03, 0:00 on December 8, 22:00 on December 11 (LST). Triangles show ending site at Beijing, called T_0 . T_{-6} , T_{-12} , T_{-18} , T_{-24} mean 6, 12, 18, 24 hours before arriving at ending site. The red lines refer to backward trajectories and the solid shaded circles represent the geometric mean particle size (GMD, nm) labeled in color bar on the right. The number beside the solid circle is the mass ratio of coating to BC, called R_{BC} for short. The pie chart shows the region source of BC. The gray represents the local contribution, and the red represents the contribution of regional transport. The blacklines refer to the distribution of number concentration.

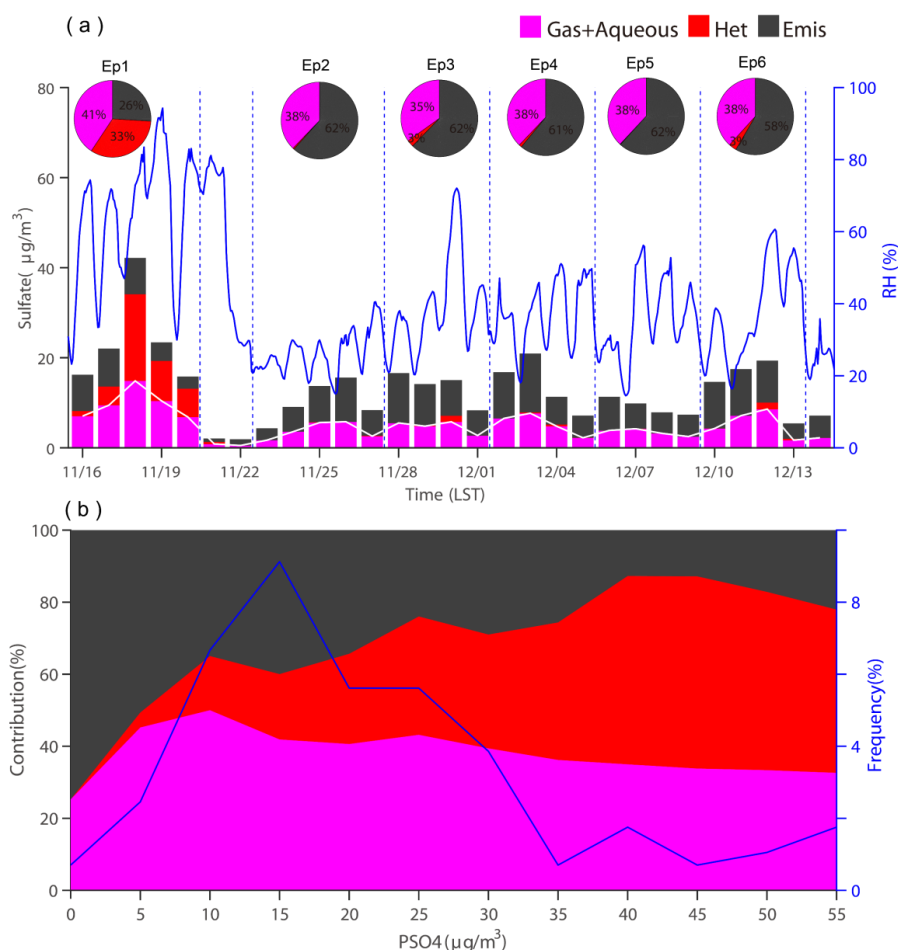


Figure 13. Contribution of different ways of sulfate formation in Beijing. (a) Daily average. Blue line shows relative humidity at Beijing. Pies show average contribution of different ways during each episode. (b) Relationship between sulphate concentration and different pathways of sulphate formation during Ep1.

Tables

Table 1. Source-tagging regions and primary $\text{PM}_{2.5}$ emissions during 15 November–15 December, 2016 in this study.^a

Regions	Descriptions	Area 10^3 km^2	Population 10^6	GDP ^b (10^{12} CNY)	Emission ^c (10^9 g)
BJ	Beijing	16.4	21.7	2.5	3.6
TJ	Tianjin	11.9	15.6	1.8	3.9
NHB	Chengde, Zhangjiakou and	84.1	11.6	0.4	3.6



		Qinhuangdao				
BTH	WHB	Baoding and Shijiazhuang	38.0	21.2	0.9	8.1
	EHB	Tangshan, Langfang and Cangzhou	33.9	20.3	1.1	10.1
	SHB	Hengshui, Xingtai and Handan	33.3	22.9	0.7	6.8
HN		Henan	167.0	95.3	4.0	26.6
SD		Shandong	155.8	99.5	6.8	38.5
SX		Shanxi	156.7	36.8	1.3	25.9
OT		Other regions				

838 ^a Regions are shown in Fig. 1c.

839 ^b GDP unit in 2016 is Chinese Yuan (CNY) (<http://www.tjcn.org/tjgb/>).

840 ^c PM_{2.5} emissions data are obtained from the 2016 Multi-resolution Emission Inventory for China

841 (MEIC) with 0.25° × 0.25° resolution.